

# Emergent interacting spin islands in a depleted strong-leg Heisenberg ladder

D. Schmidiger,<sup>1,\*</sup> K. Yu. Povarov,<sup>1</sup> S. Galeski,<sup>1</sup> N. Reynolds,<sup>1,†</sup>  
R. Bewley,<sup>2</sup> T. Guidi,<sup>2</sup> J. Ollivier,<sup>3</sup> and A. Zheludev<sup>1,‡</sup>

<sup>1</sup>*Neutron Scattering and Magnetism, Laboratory for Solid State Physics, ETH Zürich, CH-8093 Zürich, Switzerland*

<sup>2</sup>*ISIS Facility, Rutherford Appleton Laboratory, Chilton, Didcot, Oxon OX11 0QX, United Kingdom*

<sup>3</sup>*Institut Laue-Langevin, 6 rue Jules Horowitz, 38042 Grenoble, France*

(Dated: March 2, 2016)

Properties of the depleted Heisenberg spin ladder material series  $(\text{C}_7\text{H}_{10}\text{N})_2\text{Cu}_{1-z}\text{Zn}_z\text{Br}_4$  have been studied by the combination of magnetic measurements and neutron spectroscopy. Disorder-induced degrees of freedom lead to a specific magnetic response, described in terms of emergent strongly interacting “spin island” objects. The structure and dynamics of the spin islands is studied by high-resolution inelastic neutron scattering. This allows to determine their spatial shape and to observe their mutual interactions, manifested by strong spectral in-gap contributions.

PACS numbers: 75.10.Jm, 75.10.Kt, 75.40.Gb, 75.40.Mg, 75.50.-y

In the solid state, even weak perturbations may lead to qualitatively new physics described in terms of entirely new emergent degrees of freedom and quasiparticles [1]. One such perturbation, known to open the door to a variety of novel and competing ground states and rich phase diagrams, is structural or chemical disorder [2]. An exciting example of disorder-induced emergent degrees of freedom are the *magnetic* objects that appear upon the introduction of *non-magnetic* impurities in gapped quantum-disordered antiferromagnets (AFs) [3–8]. These entities may be understood as spins released from non-magnetic AF singlets by removing their partner spins. The short-range correlations in the underlying quantum AF spread these spin degrees of freedom over extended regions (“spin-islands”) around each impurity site [3]. The size of the spin islands is controlled by the correlation length in the parent system, and may be as large as dozens of nanometers. Due to their partial overlap, these spin islands interact. The original quantum AF thus acts as a “medium” that hosts a new magnetic system of *mesoscopic* objects and carries interactions between them. Due to these interactions, the emergent system may have its own unique correlations and dynamics.

The impurity-induced formation of localized  $S = 1/2$  spin objects has been thoroughly studied in gapped  $S = 1$  Haldane spin chains [4, 9–13]. Unfortunately, in these highly one-dimensional chain materials, each impurity completely severs the host system. The emergent spin islands located at the chain segment ends merely pair up into isolated dimers [4], and have no collective dynamics. This is in contrast to expectations for Heisenberg spin ladders, which are composed of *two* neighboring chains linked by rung interactions  $J_\perp$ . Within this topology, the non-magnetic impurities have a low chance to disrupt the continuity of the system and a finite-size segment typically contains a large number of mutually interacting islands. To date, the study of non-magnetic impurities in spin ladders was limited to rather complex materials with prohibitively large energy scales, such as

$\text{Sr}(\text{Cu}_{1-z}\text{Zn}_z)_2\text{O}_3$  [14] or  $\text{Bi}(\text{Cu}_{1-z}\text{Zn}_z)_2\text{PO}_6$  [5]. These cases are difficult to describe theoretically, as they involve additional interactions such as cyclic exchange, frustration, or 3D coupling. What is missing is an experimental study of emergent and interacting spin islands in a *clean* realization of the spin ladder model, such that could be compared to theoretical calculations at the quantitative level. Fortunately, in recent years, a number of new exceptionally good organic spin ladder compounds were discovered [15]. Among them,  $(\text{C}_7\text{H}_{10}\text{N})_2\text{CuBr}_4$  (DIMPY) [16, 17] realizes the rare case of a strong-leg spin ladder, which is of special interest in the context of the present study. Its dominant leg interactions imply a significant correlation length and hence significant interactions between emerging spin objects, even at low concentration. In the present Letter we show that DIMPY, diluted with nonmagnetic zinc, is indeed a perfect prototype for testing this physics. By combining thermodynamic and high-resolution inelastic neutron scattering experiments with numerical simulations, we are able to directly study the shape and interactions of the spin islands, and to quantitatively describe the impurity-induced *collective* response in the language of these emergent objects.

The parent material DIMPY was shown to be described by a simple Heisenberg spin-ladder Hamiltonian with  $J_\parallel = 1.42(6)$  meV along the leg and  $J_\perp = 0.82(2)$  meV (see Fig. 1) [17–19] and with exceptionally weak additional interactions [20–22]. We were able to chemically introduce non-magnetic impurities by replacing a fraction  $z$  of magnetic  $S = 1/2$   $\text{Cu}^{2+}$  by non-magnetic  $\text{Zn}^{2+}$  ions [23]. The magnetic susceptibility and isothermal magnetization data are presented in Fig. 2, as measured on a series of  $(\text{C}_7\text{H}_{10}\text{N})_2\text{Cu}_{1-z}\text{Zn}_z\text{Br}_4$  single crystals with varying impurity concentration  $z$  [24]. While the susceptibility of the  $z = 0$  parent compound is being dominated by a spectral gap of  $\Delta = 0.33$  meV and exponentially decays to zero at low temperatures, the susceptibility of the Zn-diluted material acquires an

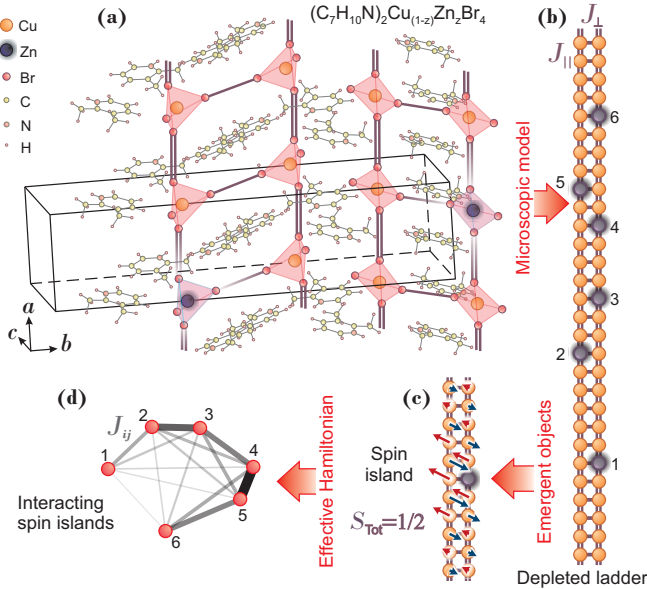


FIG. 1. From a real material to the microscopic model and then, to the effective description in terms of emergent objects. (a) The crystal structure of  $(C_7H_{10}N)_2Cu_{1-z}Zn_zBr_4$ . (b) Spin ladder model microscopic description. The random replacement of magnetic  $Cu^{2+}$  by non-magnetic  $Zn^{2+}$  renders some  $S = 1/2$  sites missing. (c) Emerging local spin degrees of freedoms (spin islands), pinned to the impurity position but with a magnetization profile extending over many unit cells. (d) Effective spin island Hamiltonian (4) with interactions controlled by the mutual distances as given by Eq. (2).

additional paramagnetic-like contribution, progressively increasing with the impurity concentration. This behavior becomes even more apparent in the low-temperature magnetization (Fig. 2b). The latter remains suppressed by the gap below the critical field of  $H_c \simeq 2.7$  T [17] in the clean material but acquires an impurity-induced contribution in the Zn-substituted derivatives. Nonetheless, the observed response is not simply described by the  $S = 1/2$  Brillouin function, as it would in case of free magnetic moments [25]. While deviations from the Brillouin function are small at low impurity concentrations, they become up to 45% at  $z = 0.06$ . Qualitatively, this is explained by the mean impurity distance  $\bar{L}_x(z) = (1-z)/(2z-z^2)$  [26] which is as large as 50 unit cells for  $z = 0.01$  but becomes comparable to the correlation length  $\xi \approx 6.3$  [24] at  $z = 0.06$ . The probability of finding close and strongly interacting islands thus rapidly increases with impurity concentration.

As a first step, we compare our measurements to numerical calculations [24] based on the full parent spin ladder Hamiltonian [17], depleted with randomly placed non-magnetic sites (Fig. 1b). Following Ref. [26], we calculate the susceptibility and magnetization with Quantum Monte Carlo (QMC) simulations of ladder systems with  $L = 500$  rungs,  $N = 2Lz$  randomly placed non-magnetic sites and averaged over 300 random impurity

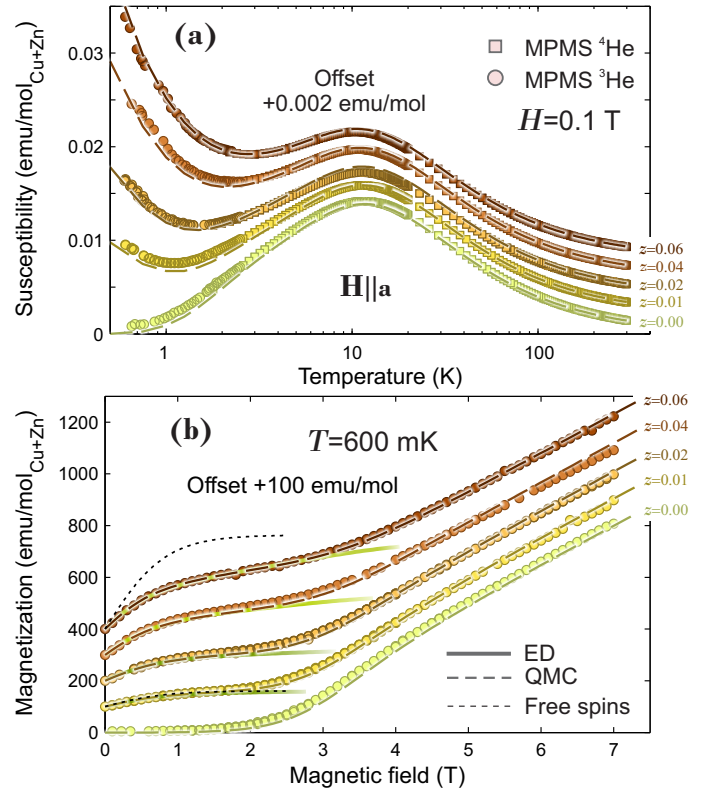


FIG. 2. Magnetization experiments on the depleted spin-ladder series  $(C_7H_{10}N)_2Cu_{1-z}Zn_zBr_4$ . (a) Susceptibility as a function of temperature. (b) Isothermal magnetization at  $T = 600$  mK for the same samples. Symbols are the experimental data. Numerical QMC simulations and results from the diagonalization of the effective model [Eq. (4)] are shown as dashed and solid lines correspondingly. Dotted lines in (b) illustrate the free-spin response for  $z = 0.01$  and  $z = 0.06$  cases.

configurations [27]. The numeric results (dashed lines in Fig. 2) quantitatively reproduce the measured data in the entire temperature- and field-range. This proves not only that we are able to chemically control the zinc concentration but also that its introduction does not lead to significant local distortion effects altering the superexchange interactions.

Extensive QMC calculations of large depleted systems, averaged over hundreds of configurations, are expensive, time-consuming and yield little physical insight. An alternative, much simpler approach is provided by the effective low-energy description in terms of interacting spin islands (Fig. 1c,d) [3, 26]. The latter are represented by  $S = 1/2$  spins  $\mathbf{S}_I$  at random impurity positions  $\mathbf{I}$ , interacting with distance-dependent effective interactions  $J^{\text{eff}}(\mathbf{L})$  and described by the Hamiltonian [26]

$$H_{\text{Sp,Is.}} = \sum_{\mathbf{I}, \mathbf{J}} J^{\text{eff}}(\mathbf{I} - \mathbf{J}) \mathbf{S}_I \cdot \mathbf{S}_J - g\mu_B H \sum_{\mathbf{I}} S_I^z, \quad (1)$$

with  $\mu_B$  and  $g$  being the Bohr magneton and the electron

$g$ -factor. Mutual spin-island interactions are mediated by the spin correlations in the hosting ladder medium. Since the latter are short-ranged, effective interactions exponentially decay with distance. In addition, due to their antiferromagnetic nature,  $J^{\text{eff}}(\mathbf{L})$  are ferro- or antiferromagnetic, depending on whether the mutual interaction path contains an odd or even number of sites [3, 26], reminiscent of the oscillatory Ruderman-Kittel-Kasuya-Yosida (RKKY) interaction [28]. Being fully controlled by the spin ladder medium, the effective interactions can be numerically obtained from a system with two non-magnetic sites at distance  $\mathbf{L}$  in a long ladder system. Following Refs. [3, 26] we have performed Matrix Product State calculations [27, 29] and confirmed that  $J^{\text{eff}}(\mathbf{L})$  is described by the simple law

$$J^{\text{eff}}(\mathbf{L}) = J_0(-1)^{L_x+L_y+1}e^{-|L_x|/\xi} \quad (2)$$

with the energy scale  $J_0 = 0.441$  meV and the decay length  $\xi = 6.28$  for the exchange constants of DIMPY [24]. By including the numerically calculated effective interactions, Eq. (4) becomes a *parameter-free* description of the emergent spin island system.

The magnetization and susceptibility of the effective model were determined [24] by exactly diagonalizing (ED) the Hamiltonian in Eq. (4), for a system of  $N = 12$  sites  $S_{\mathbf{I}}$ , randomly placed on a ladder with  $L = N/2z$  rungs and with the effective interactions given by Eq. (2). The magnetization, averaged over 5000 random configurations, is in excellent agreement with measured data (Fig. 2b). Notably, a model described by not more than 12 mutually interacting spin operators is sufficient to model the entire thermodynamic response of this complex disordered many-body quantum system. Nevertheless, the description in terms of Eq. (4) remains valid only as long as the mutual interactions controlled by the spin island correlations do not change. While the latter remain unaffected by temperature and applied field as long as the spin ladder remains in its quantum disordered regime, they fundamentally change once the system crosses the critical field  $H_c \simeq 2.7$  T [17] to the quantum critical Tomonaga-Luttinger spin liquid (TLSL) state. Above  $H_c$  the effective description naturally fails.

So far, we have successfully described the measured thermodynamic properties in terms of an effective model of emergent spin island. However, can such objects and their interactions be observed directly? To answer this question, we present a series of high-resolution inelastic neutron scattering experiments enabling to access the spectral properties of both the spin ladder medium and the low-energy spin island system. In Fig. 3a,c, we show the background-subtracted magnetic neutron spectrum of  $(\text{C}_7\text{D}_{10}\text{N})_2\text{Cu}_{0.96}\text{Zn}_{0.04}\text{Br}_4$ , as measured with the neutron time-of-flight (TOF) technique (LET spectrometer [30], ISIS facility, U.K.). Data was gathered in distinct low- and high-resolution setups with incident

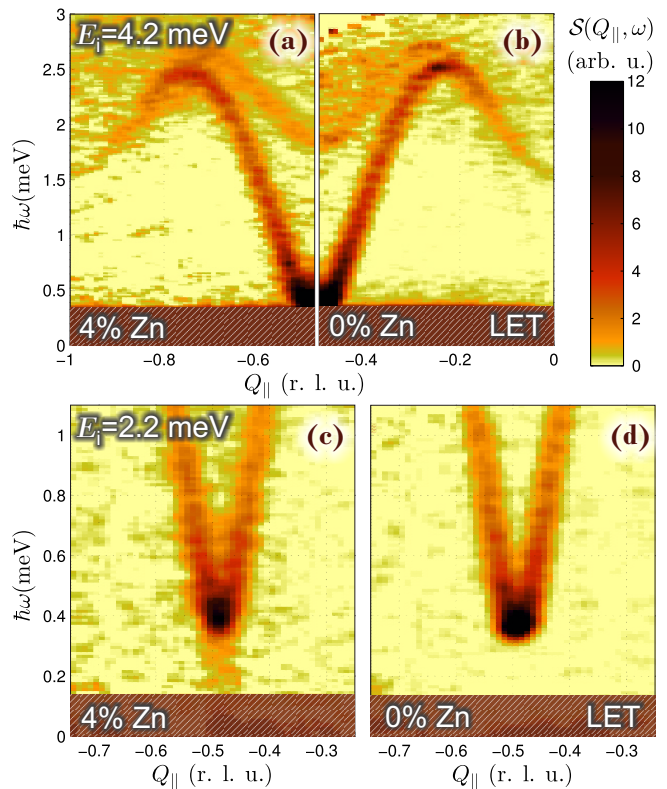


FIG. 3. Inelastic neutron scattering data on the depleted and clean spin ladder DIMPY, measured on LET instrument. (a,b) Entire spectrum in the lower resolution mode (incident energy  $E_i = 4.2$  meV). (c,d) Low-energy sector in the higher resolution mode ( $E_i = 2.2$  meV). Background corrected magnetic neutron scattering intensity is shown as a function of energy transfer  $\hbar\omega$  and momentum transfer along the leg  $Q_{\parallel}$ . Hatched regions are contaminated by parasitic nuclear incoherent scattering.

energies  $E_i = 4.2$  meV and 2.2 meV ( $T = 75$  mK). Neutron intensity is shown as a function of energy transfer  $\hbar\omega$  and momentum transfer  $Q_{\parallel} = \mathbf{Q} \cdot \mathbf{a}$  along the leg direction. Corresponding data from the parent compound is shown in Figs. 3b,d, measured under identical experimental conditions [19] and treated in the same way.

First, we observe that the properties of the spin ladder medium hosting the spin island system remains nearly unaffected by the presence of impurities (Fig. 3a,b). In both the parent and disordered compound, identical gapped and dispersive magnon and two-magnon bound state branches [17] are observed. In contrast, clear changes are found in the low-energy sector (Fig. 3c,d). The magnon gap is slightly shifted from  $\Delta = 0.33$  to 0.41 meV, reminiscent of the magnon blue-shift observed in 1D quantum-disordered AFs at finite temperature [31]. However, as a main feature, we observe a stripe of enhanced in-gap intensity developing around  $Q_{\parallel} = 0.5$  r.l.u. in the disordered compound. This contribution originates in strongly interacting spin islands, leading to a

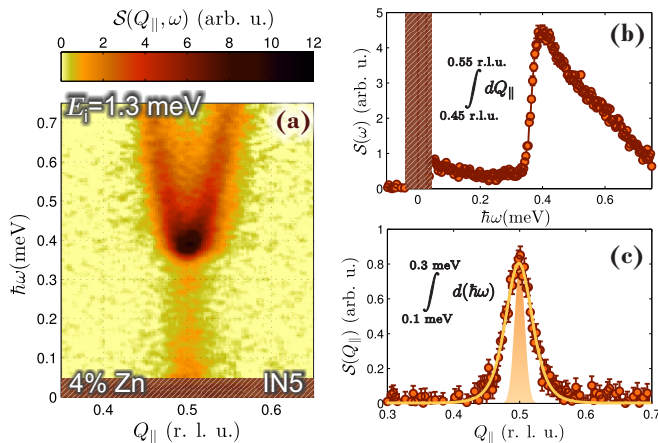


FIG. 4. Inelastic neutron scattering data on the disordered DIMPY, measured on IN5 instrument. (a) Background subtracted spectrum measured with  $E_i = 1.3$  meV. Neutron intensity is shown as a function of energy transfer  $\hbar\omega$  and momentum transfer  $Q_{\parallel}$ . (b) Neutron intensity as a function of  $\hbar\omega$  for  $Q_{\parallel}$  between 0.45 and 0.55 r.l.u. Data in the hatched area is contaminated by parasitic nuclear incoherent scattering. (c) Scattering intensity as a function of  $Q_{\parallel}$ , after integrating in  $0.1 \text{ meV} \leq \hbar\omega \leq 0.3 \text{ meV}$ . Instrumental resolution (shaded area) is shown along with the resolution-convoluted fit (3) [solid line].

disorder-induced finite density of states inside the gap.

It is even more pronounced in the spectrum presented in Fig. 4a, measured with a lower incident energy of  $E_i = 1.3$  meV and thus better resolution (IN5 instrument [32], ILL, France). The spin island contribution progressively increases with decreasing energy  $\hbar\omega$ , as shown in Fig. 4b. This is readily explained since at  $z = 0.04$ , the probability of finding spin islands only weakly interacting with others remains large and there is a vast number of quantum states at low energies.

As a main characteristics, these in-gap contributions exhibit an intrinsic  $Q_{\parallel}$  linewidth, as shown in Fig. 4c. This intrinsic linewidth is a measure of the spin island real-space magnetization profile. Similar to conventional magnetic neutron scattering [33], where intensity is modulated by the magnetic form factor (the Fourier transform of the magnetic ions' unpaired electron density), scattering by spin islands is modulated by the square of the spin island form factor  $F(Q_{\parallel}, Q_{\perp})$  — the Fourier transform of its real space shape. A similar reasoning was applied to determine the spatial shape of emergent local objects in the substantially different cases of the charge-doped or depleted Haldane spin chains  $Y_{2-z}Ca_zBaNiO_5$  [34],  $Y_2BaNi_{1-z}Mg_zO_5$  [4]. For a spin island with exponentially decaying staggered magnetization on a ladder, the form factor reads as

$$F(Q_{\parallel}, Q_{\perp}) = \frac{(1 - e^{-i2\pi Q_{\perp}}) \sinh(\xi^{-1})}{\cos(2\pi Q_{\parallel}) + \cosh(\xi^{-1})} - 1. \quad (3)$$

Here,  $\xi$  denotes the real space decay length and  $Q_{\perp}$  is

the momentum transfer along the rung [35]. We compared  $F|(Q_{\parallel}, Q_{\perp})|^2$ , averaged over  $Q_{\perp}$ , to our experimental data and by convolution with experimental resolution, we were able to quantify the real space decay length to be  $\xi = 5.0(2)$ . The magnetization profile thus decays to 10% of its initial value only after 15 unit cells and the size of an emergent spin island is of the order of 20 nm. Notably, the determined decay length is slightly shorter than the numerically calculated value of  $\xi = 6.27$  [24]. However, this is not surprising since in-gap states observed in experiments are located at a comparatively large energy transfer on the order of 0.1 meV and thus mainly originate from dimers or clusters of spin islands close to each other. Influenced by the nearby spin islands, the magnetization profile thus deviates from the one of an isolated spin island.

In conclusion, by combining thermodynamic and high-resolution inelastic neutron scattering techniques with numerical simulations, we were able to quantitatively study the properties of a system of strongly interacting spin islands formed in a strong-leg Heisenberg spin ladder depleted with non-magnetic impurities. An effective description in the language of these objects explains and quantitatively reproduces the measured data. As long as the spin-ladder medium remains quantum disordered at  $H < H_c$ , this effective description is faithful and, in principle, would allow not only to describe the thermodynamic response but even to access dynamical quantities such as time-dependent correlation functions [36]. Beyond  $H_c$ , however, the effective description breaks down due to the quantum phase transition to the TLSL state [37], rendering the spin-ladder correlation functions fundamentally different. To the authors knowledge, the problem of non-magnetic impurities and the fate of spin islands in the TLSL phase of a spin ladder or their influence on the magnetically ordered state [17, 38] has not been addressed experimentally or theoretically. We hope that our study stimulates further efforts and experiments towards understanding the impurity-induced physics in such systems.

This work is partially supported by the Swiss National Science Foundation, Division II. We would like to thank Dr. S. Mühlbauer (FRM II, Technische Universität München) for his involvement at the early stages of this project and Dr. S. Gvasaliya (ETH Zürich) for assistance with the magnetic measurements. Simulations were performed on the Brutus cluster (ETH Zürich).

\* schmdavi@phys.ethz.ch

† Present address: Laboratory for Neutron Scattering, Paul Scherrer Institut, CH-5232 Villigen, Switzerland.

‡ zhelud@ethz.ch; <http://www.neutron.ethz.ch/>

[1] P. W. Anderson, “More is different,” *Science* **177**, 393 (1972).

- [2] E. Dagotto, “Complexity in strongly correlated electronic systems,” *Science* **309**, 257 (2005).
- [3] H.-J. Mikeska, U. Neugebauer, and U. Schollwöck, “Spin ladders with nonmagnetic impurities,” *Phys. Rev. B* **55**, 2955 (1997).
- [4] M. Kenzelmann, G. Xu, I. A. Zaliznyak, C. Broholm, J. F. DiTusa, G. Aeppli, T. Ito, K. Oka, and H. Takagi, “Structure of End States for a Haldane Spin Chain,” *Phys. Rev. Lett.* **90**, 087202 (2003).
- [5] J. Bobroff, N. Laflorencie, L. K. Alexander, A. V. Mahajan, B. Koteswararao, and P. Mendels, “Impurity-Induced Magnetic Order in Low-Dimensional Spin-Gapped Materials,” *Phys. Rev. Lett.* **103**, 047201 (2009).
- [6] M. Hase, I. Terasaki, Y. Sasago, K. Uchinokura, and H. Obara, “Effects of substitution of Zn for Cu in the spin-Peierls cuprate,  $\text{CuGeO}_3$ : The suppression of the spin-Peierls transition and the occurrence of a new spin-glass state,” *Phys. Rev. Lett.* **71**, 4059–4062 (1993); M. Hase, K. Uchinokura, R. J. Birgeneau, K. Hirota, and G. Shirane, “Neutron-scattering study of magnetism in single-crystal  $\text{Cu}_{1-x}\text{Zn}_x\text{GeO}_3$ ,” *J. Phys. Soc. Jpn.* **65**, 1392–1398 (1996); K. Uchinokura, “Spin-peierls transition in  $\text{CuGeO}_3$  and impurity-induced ordered phases in low-dimensional spin-gap systems,” *J. Phys. Condens. Matter* **14**, R195 (2002).
- [7] S. Sahling, G. Remenyi, C. Paulsen, P. Monceau, V. Saligram, C. Marin, A. Revcolevschi, L. P. Regnault, and J. E. Lorenzo, “Experimental realization of long-distance entanglement between spins in antiferromagnetic quantum spin chains,” *Nature Phys.* **11**, 255 (2015).
- [8] T. Guidi, B. Gillon, S. A. Mason, E. Garlatti, S. Carretta, P. Santini, A. Stunault, R. Caciuffo, J. van Slageren, B. Klemke, A. Cousson, G. A. Timco, and R. E. P. Winpenny, “Direct observation of finite size effects in chains of antiferromagnetically coupled spins,” *Nat. Commun.* **6**, 7061 (2015).
- [9] S. H. Glarum, S. Geschwind, K. M. Lee, M. L. Kaplan, and J. Michel, “Observation of fractional spin  $S = 1/2$  on open ends of  $S = 1$  linear antiferromagnetic chains: Nonmagnetic doping,” *Phys. Rev. Lett.* **67**, 1614 (1991).
- [10] B. Batlogg, S.-W. Cheong, and L.W. Rupp Jr., “Haldane spin state in  $\text{Y}_2\text{Ba}(\text{Ni}, \text{Zn or Mg})\text{O}_5$ ,” *Physica B* **194-196**, Part 1, 173 (1994).
- [11] F. Tedoldi, R. Santachiara, and M. Horvatić, “ $^{89}\text{Y}$  NMR Imaging of the Staggered Magnetization in the Doped Haldane Chain  $\text{Y}_2\text{BaNi}_{1-x}\text{Mg}_x\text{O}_5$ ,” *Phys. Rev. Lett.* **83**, 412 (1999).
- [12] Y. Uchiyama, Y. Sasago, I. Tsukada, K. Uchinokura, A. Zheludev, T. Hayashi, N. Miura, and P. Böni, “Spin-Vacancy-Induced Long-Range Order in a New Haldane-Gap Antiferromagnet,” *Phys. Rev. Lett.* **83**, 632 (1999).
- [13] T. Masuda, K. Uchinokura, T. Hayashi, and N. Miura, “Impurity-induced antiferromagnetic phase in a doped Haldane system  $\text{Pb}(\text{Ni}_{1-x}\text{Mg}_x)_2\text{V}_2\text{O}_8$ ,” *Phys. Rev. B* **66**, 174416 (2002).
- [14] M. Azuma, Y. Fujishiro, M. Takano, M. Nohara, and H. Takagi, “Switching of the gapped singlet spin-liquid state to an antiferromagnetically ordered state in  $\text{Sr}(\text{Cu}_{1-x}\text{Zn}_x)_2\text{O}_3$ ,” *Phys. Rev. B* **55**, R8658 (1997).
- [15] C. P. Landee and M. M. Turnbull, “Recent Developments in Low-Dimensional Copper(II) Molecular Magnets,” *Eur. J. Inorg. Chem.* **2013**, 2266 (2013).
- [16] A. Shapiro, C. P. Landee, M. M. Turnbull, J. Jor-net, M. Deumal, J. J. Novoa, M. A. Robb, and W. Lewis, “Synthesis, Structure, and Magnetic Properties of an Antiferromagnetic Spin-Ladder Complex: Bis(2,3-dimethylpyridinium) Tetrabromocuprate,” *J. Am. Chem. Soc.* **129**, 952 (2007).
- [17] D. Schmidiger, P. Bouillot, S. Mühlbauer, S. Gvasaliya, C. Kollath, T. Giamarchi, and A. Zheludev, “Spectral and thermodynamic properties of a strong-leg quantum spin ladder,” *Phys. Rev. Lett.* **108**, 167201 (2012).
- [18] D. Schmidiger, P. Bouillot, T. Guidi, R. Bewley, C. Kollath, T. Giamarchi, and A. Zheludev, “Spectrum of a magnetized strong-leg quantum spin ladder,” *Phys. Rev. Lett.* **111**, 107202 (2013).
- [19] K. Yu. Povarov, D. Schmidiger, N. Reynolds, R. Bewley, and A. Zheludev, “Scaling of temporal correlations in an attractive Tomonaga-Luttinger spin liquid,” *Phys. Rev. B* **91**, 020406 (2015).
- [20] M. Jeong, H. Mayaffre, C. Berthier, D. Schmidiger, A. Zheludev, and M. Horvatić, “Attractive Tomonaga-Luttinger Liquid in a Quantum Spin Ladder,” *Phys. Rev. Lett.* **111**, 106404 (2013).
- [21] V. N. Glazkov, M. Fayzullin, Yu. Krasnikova, G. Skoblin, D. Schmidiger, S. Mühlbauer, and A. Zheludev, “ESR study of the spin ladder with uniform Dzyaloshinskii-Moriya interaction,” *Phys. Rev. B* **92**, 184403 (2015).
- [22] M. Ozerov, M. Maksymenko, J. Wosnitza, A. Honecker, C. P. Landee, M. M. Turnbull, S. C. Furuya, T. Giamarchi, and S. A. Zvyagin, “Electron spin resonance modes in a strong-leg ladder in the Tomonaga-Luttinger liquid phase,” *Phys. Rev. B* **92**, 241113 (2015).
- [23] T. Yankova, D. Hüvonen, S. Mühlbauer, D. Schmidiger, E. Wulf, S. Zhao, A. Zheludev, T. Hong, V. O. Garlea, R. Custelcean, and G. Ehlers, “Crystals for neutron scattering studies of quantum magnetism,” *Philos. Mag.* **92**, 2629 (2012).
- [24] “Supplementary material,”
- [25] R. M. White, *Quantum Theory of Magnetism, Magnetic Properties of Materials*, 3rd ed. (Springer-Verlag, Berlin, Heidelberg, New York, 2007).
- [26] A. Lavaré, G. Roux, and N. Laflorencie, “Magnetic responses of randomly depleted spin ladders,” *Phys. Rev. B* **88**, 134420 (2013).
- [27] B. Bauer, L. D. Carr, H. G. Evertz, A. Feiguin, J. Freire, S. Fuchs, L. Gamper, J. Gukelberger, E. Gull, S. Guertler, *et al.*, “The ALPS project release 2.0: open source software for strongly correlated systems,” *J. Stat. Mech. Theor. Exp.* **2011**, P05001 (2011).
- [28] M. A. Ruderman and C. Kittel, “Indirect Exchange Coupling of Nuclear Magnetic Moments by Conduction Electrons,” *Phys. Rev.* **96**, 99 (1954); T. Kasuya, “A Theory of Metallic Ferro- and Antiferromagnetism on Zener’s Model,” *Prog. Theor. Phys.* **16**, 45 (1956); K. Yosida, “Magnetic Properties of Cu-Mn Alloys,” *Phys. Rev.* **106**, 893 (1957).
- [29] M. Dolfi, B. Bauer, S. Keller, A. Kosenkov, T. Ewart, A. Kantian, T. Giamarchi, and M. Troyer, “Matrix product state applications for the ALPS project,” *Comput. Phys. Commun.* **185**, 3430 (2014).
- [30] R.I. Bewley, J.W. Taylor, and S.M. Bennington., “LET, a cold neutron multi-disk chopper spectrometer at ISIS,” *Nucl. Instr. Meth. Phys. Res. A* **637**, 128 (2011).
- [31] A. Zheludev, V. O. Garlea, L.-P. Regnault, H. Manaka, A. Tsvetlik, and J.-H. Chung, “Extended Universal Finite- $T$  Renormalization of Excitations in a Class of

- One-Dimensional Quantum Magnets,” *Phys. Rev. Lett.* **100**, 157204 (2008).
- [32] J. Ollivier and H. Mutka, “IN5 Cold Neutron Time-of-Flight Spectrometer, Prepared to Tackle Single Crystal Spectroscopy,” *J. Phys. Soc. Jpn.* **80**, SB003 (2011).
- [33] G. L. Squires, *Introduction to the Theory of Thermal Neutron Scattering* (Cambridge University Press, Cambridge, London, New York, Melbourne, 1978).
- [34] G. Xu, G. Aeppli, M. E. Bisher, C. Broholm, J. F. DiTusa, C. D. Frost, T. Ito, K. Oka, R. L. Paul, H. Takagi, and M. M. J. Treacy, “Holes in a quantum spin liquid,” *Science* **289**, 419 (2000).
- [35] D. Schmidiger, S. Mühlbauer, S. N. Gvasaliya, T. Yankova, and A. Zheludev, “Long-lived magnons throughout the Brillouin zone of the strong-leg spin ladder  $(\text{C}_7\text{H}_{10}\text{N})_2\text{CuBr}_4$ ,” *Phys. Rev. B* **84**, 144421 (2011).
- [36] D. Schmidiger, Unpublished.
- [37] T. Giamarchi, *Quantum physics in One Dimension* (Oxford university press, Oxford, 2004).
- [38] T. Giamarchi, C. Rüegg, and O. Tchernyshyov, “Bose-Einstein condensation in magnetic insulators,” *Nature Phys.* **4**, 198 (2008).

# Supplementary material: Emergent interacting spin islands in a depleted strong-leg Heisenberg ladder

## (A) EXPERIMENTAL DETAILS

### Measurement details

Single crystals of  $(\text{C}_7\text{H}_{10}\text{N})_2\text{Cu}_{1-z}\text{Zn}_z\text{Br}_4$  were grown from solution by the temperature gradient method [1], according to the same procedure as for the original material  $(\text{C}_7\text{H}_{10}\text{N})_2\text{CuBr}_4$  [2] but with replacement of the relevant amount  $z$  of  $\text{CuBr}_2$  by  $\text{ZnBr}_2$ . For the magnetic measurements single crystals with typical masses of 15 mg were used. The measurements were carried out with the help of a standard Quantum Design Magnetic Properties Measurement System (MPMS-XL SQUID magnetometer). For measurements below 1.7 K, the  $^3\text{He}$  cryostat insert for MPMS (iQuantum iHelium3) was employed. For all the samples, the magnetic field was applied along the  $a$  axis of the structure.

For the synthesis of single crystals for neutron scattering, all the hydrogen-containing chemicals were replaced by the deuterated analogues. Similar to our studies on the clean material [3–7], the measured sample was composed of three co-aligned crystals of  $(\text{C}_7\text{D}_{10}\text{N})_2\text{Cu}_{0.96}\text{Zn}_{0.04}\text{Br}_4$  with typical masses of 800 mg each. They were fixed on a similar aluminum sample holder as previously used (see e. g. Fig. 2 of Ref. [1]), with the  $b$  direction being vertical.

### Spin island scattering in reciprocal space

Hereby, we would like to provide an additional figure, showing the part of reciprocal space accessed in the IN5 neutron experiment as well as the 1D spin island scattering.

Data in Fig. 1 (measured with the IN5 instrument [8], with  $E_i = 1.3$  meV and  $T = 75$  mK) was integrated along the out-of-plane direction  $-1 \text{ r.l.u.} \leq Q_k \leq 1 \text{ r.l.u.}$  and in the energy range  $0.1 \text{ meV} \leq \hbar\omega \leq 0.3 \text{ meV}$ . The spin island scattering is readily observed as a stripe of intensity, located at  $Q_{\parallel} = 0.5 \text{ r.l.u.}$ .

## (B) NUMERICAL DETAILS

In this section, further details about the numerical simulations are provided. We follow closely the previous work [9, 10], studying the general  $J_{\parallel} = J_{\perp}$  coupling case.

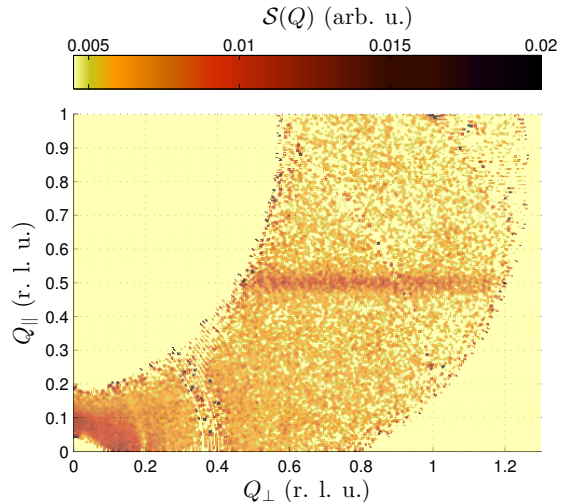


FIG. 1. Neutron intensity of  $(\text{C}_7\text{D}_{10}\text{N})_2\text{Cu}_{1-z}\text{Zn}_z\text{Br}_4$  with  $z = 0.04$ , as measured with  $E_i = 1.3$  meV and  $T = 75$  mK. Uncorrected data is shown as a function of  $Q_{\parallel}$  (along the ladder leg) and the perpendicular in-plane direction. Data was integrated in the out-of-plane direction  $Q_k$  ( $-1 \text{ r.l.u.} \leq Q_k \leq 1 \text{ r.l.u.}$ ) and in the energy range  $0.1 \text{ meV} \leq \hbar\omega \leq 0.3 \text{ meV}$ .

### Magnetization profile

The shape of the emergent magnetization profile around an impurity was studied by placing a single  $S = 0$  site in the center of a ladder with  $2 \times 150$  spins and by calculating the local magnetization  $\langle S_i^z \rangle$  of the ground state with  $M_S = 1/2$ . Fig. 2 illustrates the obtained local magnetization  $\langle S_i^z \rangle$  using the Density Matrix Renormalization Group (DMRG) algorithm from the ALPS libraries [11] ( $J_{\parallel} = 1.42$  meV and  $J_{\perp} = 0.82$  meV, 350 DMRG states kept). The local magnetization follows an exponential law without further corrections as expected [9, 10]. By fitting  $\log |\langle S_i^z \rangle|$  with a linear function, the exponential decay length was determined to be  $\xi = 6.27(1)$ .

The spin island form factor  $F(Q_{\parallel}, Q_{\perp})$  is obtained by Fourier transformation,

$$F(Q_{\parallel}, Q_{\perp}) = \sum_{n=-\infty}^{\infty} \sum_{m=0}^1 S_{n,m} e^{i2\pi n Q_{\parallel}} e^{im2\pi Q_{\perp}}, \quad (1)$$

and with  $S_{n,m} \approx S(-1)^{n+m} e^{-|n|/\xi}$  and  $S_{0,0} = 0$  at the impurity site, the latter simplifies to

$$F(Q_{\parallel}, Q_{\perp}) = \frac{(1 - e^{-i2\pi Q_{\perp}}) \sinh(\xi^{-1})}{\cos(2\pi Q_{\parallel}) + \cosh(\xi^{-1})} - 1. \quad (2)$$

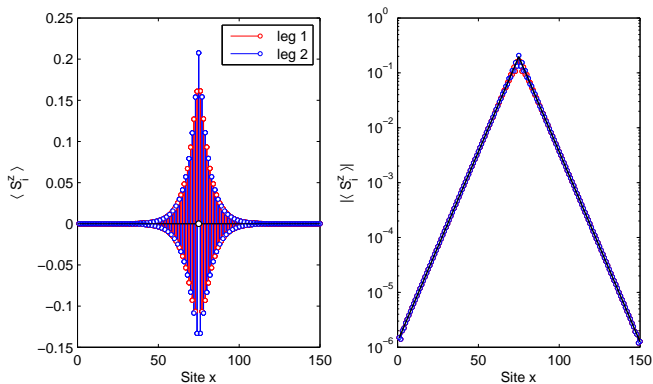


FIG. 2. Local magnetization  $\langle S_i^z \rangle$  of a spin ladder with a single non-magnetic impurity in the center as calculated with the DMRG method ( $J_{\parallel} = 1.42$  meV and  $J_{\perp} = 0.82$  meV). Linear (left panel) and logarithmic (right panel) visualization, together with the exponential fit (solid line).

### Effective interactions

If two impurities are introduced, two spin islands emerge, represented by effective spins  $\mathbf{S}_{\mathbf{I}}$  at the impurity sites, with  $S_{\mathbf{I}} = 1/2$  [10]. Their interaction depends on the distance along the leg ( $L_x$ ) and rung ( $L_y$ ) and due to their effective interaction, they pair up to a dimer with a  $S = 0$  singlet and a  $S = 1$  triplet state at energies well below the gap energy of the ladder system [9, 10]. Depending on whether  $L_x + L_y$  is odd or even, the effective interaction is ferro- or antiferromagnetic (FM or AFM). The mutual effective interactions were determined based on Matrix Product State (MPS) [12] calculations of ladder systems with  $2 \times 150$  sites and two non-magnetic impurities placed at a predefined distance  $L_x$  along the leg and either in 'cis' or 'trans' configuration (impurities on the same leg or different legs [9]). The two impurities were centered around the middle of the ladder. In order to minimize boundary effects, the distance to the ladder ends is larger than 4-5 correlation lengths. Following the approach described in Refs. [9, 10], the two lowest energies in the symmetry sectors with total spin projection of  $M_S = 0$  and  $M_S = 1$  were calculated. If spin-island interactions are AFM, the lowest state corresponds to a singlet ( $S = 0$ ,  $M_S = 0$ ) while the first excited state is a triplet ( $S = 1$ ,  $M_S = 0, \pm 1$ ) and vice versa for FM interactions. The energy difference between the lowest two states in the  $M_S = 0$  sector thus corresponds to  $J^{\text{eff}}(\mathbf{L})$  while the sign is determined from the lowest energy state of the  $M_S = 1$  sector, as discussed in Refs. [9, 10].

Calculations were performed with the matrix MPS algorithm from the ALPS package [12] (250 states kept). As an independent check-up, the results published in table II of Ref. [9] were successfully reproduced first. In the latter, a similar numerical study was performed for the  $J_{\text{leg}}/J_{\text{rung}} = 1$  coupling case, close to the DIMPY

coupling ratio of 1.73.

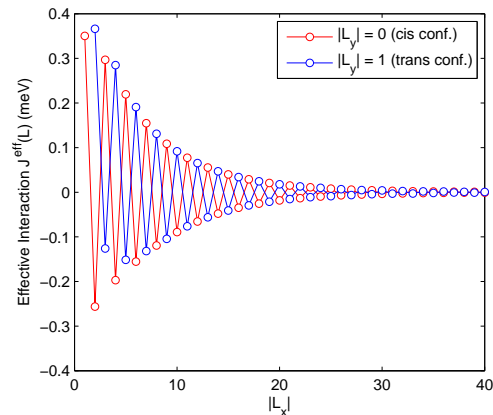


FIG. 3. Effective interactions  $J^{\text{eff}}(\mathbf{L})$  obtained based on DMRG calculations of two non-magnetic sites placed in the center of a spin ladder with a mutual distance  $\mathbf{L} = (L_x, L_y)$ , as described in the text. Red and blue symbols correspond to non-magnetic sites at the same or different legs (with  $L_y = 0$  and  $|L_y| = 1$  respectively).

The determined effective interactions are shown in Fig. 3. As previously noted in Refs. [9, 10], they follow

$$J^{\text{eff}}(\mathbf{L}) = J_0 (-1)^{L_x + L_y + 1} e^{-|L_x|/\xi} \quad (3)$$

where  $L_x \in \mathbb{Z}$  and  $L_y \in \{0, 1\}$ . The parameters  $J_0$  and  $\xi$  were determined to be  $J_0 = 0.441(7)$  meV and  $\xi = 6.28(3)$  unit cells for the DIMPY coupling case, in agreement with the trend shown in Fig. 2 and Fig. 5 of Ref. [10].

### Thermodynamics: QMC calculations

Since the original Heisenberg spin ladder Hamiltonian is non-frustrated, the thermodynamic properties are accessible with numerical Quantum Monte Carlo (QMC) calculations. The temperature-dependent susceptibility  $\chi(T)$  and the magnetization  $M(T, H)$  were calculated using the QMC algorithms provided by the ALPS package [11]. Calculations were performed for  $J_{\parallel} = 1.42$  meV and  $J_{\perp} = 0.82$  meV, on depleted ladders with  $2 \times 500 = 1000$  sites and a fixed number  $N = z \cdot 1000$  of randomly placed non-magnetic sites. Similar to Ref. [10], all thermodynamic quantities were averaged over 300 random configurations (total computation time: 2 months, parallelized to 32-64 cores on the Brutus Cluster at ETH Zürich). The susceptibility was calculated using the 'loop' algorithm, for  $0.5 \text{ K} \leq T \leq 300 \text{ K}$  (Fig. 4, coloured symbols in upper panel). The field-dependent magnetization was calculated as a function of magnetic field, for  $0 \text{ T} \leq H \leq 8 \text{ T}$ , for  $T = 0.6 \text{ K}$  (Fig. 4, coloured symbols in lower panel). For the latter, the Stochastic Series Ex-

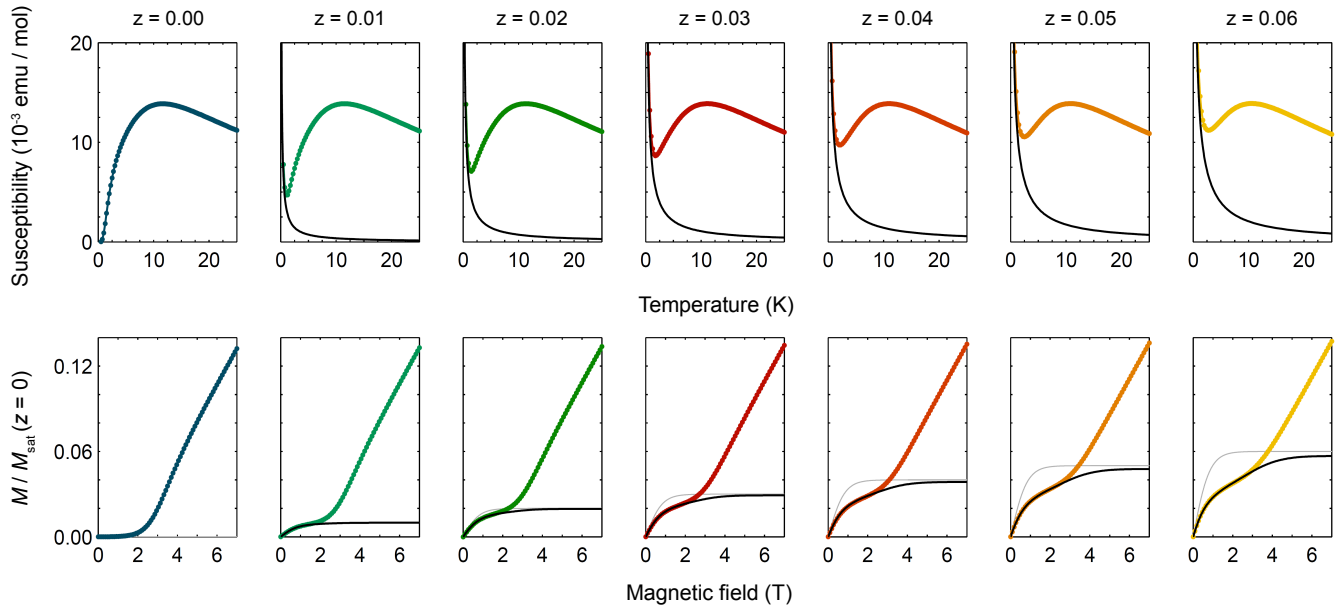


FIG. 4. Summary of numerical calculations of zero-field susceptibility  $\chi(T)$  (upper panel) and field-dependent magnetization  $M(T, H)$  at  $T = 600$  mK (lower panel), performed for the coupling case of the depleted Heisenberg spin ladder  $(\text{C}_7\text{H}_{10}\text{N})_2\text{Cu}_{1-z}\text{Zn}_z\text{Br}_4$  with  $z \leq 0.06$ . Magnetization is normalized with respect to the magnetization of the pure  $z = 0$  model and thus corresponds to  $2\langle S_i^z \rangle$ , averaged over all magnetic and non-magnetic sites. Coloured symbols: QMC calculations of the full Hamiltonian with  $N = 2Lz$  non-magnetic sites and  $L = 500$  rungs, averaged over 300 random configurations. Black lines: Exact diagonalization of the low-energy effective model, as described in the text, with  $N = 12$  spin islands  $\mathbf{S}_\mathbf{I}$  and 5000 random configurations. Gray line: Brillouin response assuming that each non-magnetic impurity is accompanied by a spin island and without interactions between different spin islands.

pansion (SSE) algorithm with directed loops [11, 13] was applied, similar to Ref. [10].

### Thermodynamics: Effective model

The low-energy model is described by effective  $S = 1/2$  spin operators at the site of impurities describing the spin islands, interacting through [10]

$$\mathcal{H}_{\text{Sp.Is.}} = \sum_{\mathbf{I}, \mathbf{J}} J^{\text{eff}}(\mathbf{I} - \mathbf{J}) \mathbf{S}_\mathbf{I} \cdot \mathbf{S}_\mathbf{J} - g\mu_B H \sum_{\mathbf{I}} S_\mathbf{I}^z. \quad (4)$$

Interactions  $J^{\text{eff}}(\mathbf{L})$  depend on the distances  $\mathbf{L} = (L_x, L_y)$ , as determined in the 'Effective interactions' subsection.

A small number of effective spins  $\mathbf{S}_\mathbf{I}$  was randomly placed on  $N$  non-equal positions of a ladder with  $L = N/2z$  rungs. From this random arrangement, the mutual distances  $\mathbf{L} = \mathbf{I} - \mathbf{J}$  and the corresponding interactions  $J^{\text{eff}}(\mathbf{L})$  were determined. Before setting up the Hamiltonian, two special cases were considered (Fig. 5).

First, impurities on adjacent rungs in trans position ( $|L_x| = 1$  and  $|L_y| = 1$ ) split the system into two non-interacting segments, releasing a spin island on both sides. Second, impurities on the same rung ( $L_x = 0$

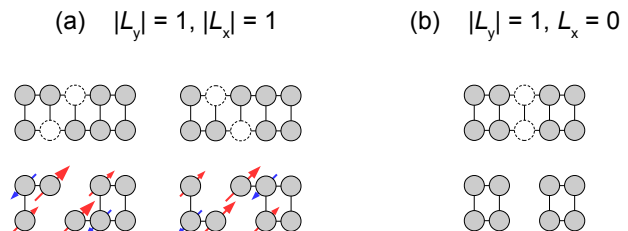


FIG. 5. Two special cases considered. (a) Impurities on adjacent rungs in trans position lead to fragmentation and release two impurities, one at each end. (b) Two impurities occupying the same rung lead to fragmentation but release no spin island at all.

and  $|L_y| = 1$ ) cut the ladder into non-interacting fragments as well. However, in contrast, the latter release no additional spin island. Based on these requirements, the Hamiltonian was set up according to Eq. (4) and by exactly diagonalizing (ED) the latter, both eigenvalues  $E_\mu$  with spin projection quantum number  $M_{S, \mu}$  and eigenvectors  $V_\mu$  were obtained. From the former, thermodynamic quantities such as the magnetization and the

susceptibility were calculated,

$$M_r(T, H) = \frac{2z}{N} \langle M \rangle$$

$$\chi_{\text{mol}}(T, H) = \frac{zN_A (g\mu_B)^2}{N k_B T} (\langle M^2 \rangle - \langle M \rangle^2) \quad (5)$$

with  $-1 \leq M_r(T, H) \leq 1$ ,  $h = g\mu_B H$  and

$$\mathcal{Z} = \sum_{\mu} \exp \left[ -\frac{E_{\mu} - h M_{S,\mu}}{k_B T} \right]$$

$$\langle M^{\alpha} \rangle = \frac{1}{\mathcal{Z}} \sum_{\mu} M_{S,\mu}^{\alpha} \exp \left[ -\frac{E_{\mu} - h M_{S,\mu}}{k_B T} \right]. \quad (6)$$

The results were averaged over many repetitions  $R$  of randomly chosen configurations of  $N$  impurities on a ladder with  $L = N/2z$  rungs.

The susceptibility and field-dependent magnetization ( $T = 0.6$  K) are shown in Fig. 4 as black lines, for different  $z$ . Calculations were performed for a fixed number of  $N = 12$  impurities randomly placed on ladders with 1200, 600, 400, 300, 240 and 200 sites for  $z = 0.01, 0.02, 0.03, 0.04, 0.05$  and  $0.06$  respectively. The result was averaged over  $R = 5000$  random configurations. By performing calculations for different number of impurities  $2 \leq N \leq 12$ , we estimate that despite the small number of impurities, the mean deviation of the thermodynamic quantities from the large- $N$  limit is less than 2% for  $z = 0.06$  and even less for  $z < 0.06$ . Calculations according to the effective model are similar to the ones published in Ref. [10] for the general  $J_{\parallel} = J_{\perp}$  case (with  $N = 10$  effective spins and  $R = 1000$  repetitions), except for the additional special cases considered in this study (Fig. 5). Notably and within the range of applicability, the agreement between the ED calculations according to the effective model and the QMC calculation of the full depleted ladder Hamiltonian is excellent, for all concentrations considered and both for the susceptibility and magnetization.

We note that the ED treatment of the effective model provides access to the eigenvectors  $V_{\mu}$  as well, thus enabling to calculate dynamical properties such as local correlations  $\mathcal{S}(\omega)$ , measurable with inelastic neutron scattering [36].

### Comparison to free spin model

Finally, it is instructive to compare the QMC and ED numerical results in Fig. 4 to the simplified model based on the naive assumption that each non-magnetic ion is accompanied by a spin island and that the latter are non interacting, thus leading to a Brillouin response (gray lines in Fig. 4)

$$\frac{M(T, H)}{M_{\text{sat}}(z = 0)} = z \tanh \left[ \frac{g\mu_B H}{2k_B T} \right]. \quad (7)$$

At very low concentration, this model becomes a faithful description since spin islands are well separated on average (mean distance  $\bar{L}_x \gg \xi$ ) and thus non-interacting. However, at  $z \gtrsim 0.02$ , the free spin model becomes inappropriate in two ways. First, interactions between mutual spin islands become progressively more important and deviations from the Brillouin response apparent. Second, the probability of impurities occupying the same rung increases as well. In the latter case (Fig. 5b), no spin island is created at all. The probability that, in a system with impurity concentration  $z$ , an impurity shares a rung with another impurity is  $p = z/2$  [10]. Since two impurities are needed to form such a non-magnetic rung pair and since both do not release a spin island, the saturated magnetic moment of the effective model is  $z(1 - z)$  instead of  $z$  as in Eq. (7).

---

\* schmdavi@phys.ethz.ch

† Present address: Laboratory for Neutron Scattering, Paul Scherrer Institut, CH-5232 Villigen, Switzerland.

‡ zhelud@ethz.ch; <http://www.neutron.ethz.ch/>

- [1] T. Yankova, D. Hüvonen, S. Mühlbauer, D. Schmidiger, E. Wulf, S. Zhao, A. Zheludev, T. Hong, V. O. Garlea, R. Custelcean, and G. Ehlers, “Crystals for neutron scattering studies of quantum magnetism,” *Philos. Mag.* **92**, 2629 (2012).
- [2] A. Shapiro, C. P. Landee, M. M. Turnbull, J. Jor-net, M. Deumal, J. J. Novoa, M. A. Robb, and W. Lewis, “Synthesis, Structure, and Magnetic Properties of an Antiferromagnetic Spin-Ladder Complex: Bis(2,3-dimethylpyridinium) Tetrabromocuprate,” *J. Am. Chem. Soc.* **129**, 952 (2007).
- [3] D. Schmidiger, S. Mühlbauer, S. N. Gvasaliya, T. Yankova, and A. Zheludev, “Long-lived magnons throughout the Brillouin zone of the strong-leg spin ladder  $(\text{C}_7\text{H}_{10}\text{N})_2\text{CuBr}_4$ ,” *Phys. Rev. B* **84**, 144421 (2011).
- [4] D. Schmidiger, P. Bouillot, S. Mühlbauer, S. Gvasaliya, C. Kollath, T. Giamarchi, and A. Zheludev, “Spectral and thermodynamic properties of a strong-leg quantum spin ladder,” *Phys. Rev. Lett.* **108**, 167201 (2012).
- [5] D. Schmidiger, S. Mühlbauer, A. Zheludev, P. Bouillot, T. Giamarchi, C. Kollath, G. Ehlers, and A. M. Tsvelik, “Symmetric and asymmetric excitations of a strong-leg quantum spin ladder,” *Phys. Rev. B* **88**, 094411 (2013).
- [6] D. Schmidiger, P. Bouillot, T. Guidi, R. Bewley, C. Kollath, T. Giamarchi, and A. Zheludev, “Spectrum of a magnetized strong-leg quantum spin ladder,” *Phys. Rev. Lett.* **111**, 107202 (2013).
- [7] K. Yu. Povarov, D. Schmidiger, N. Reynolds, R. Bewley, and A. Zheludev, “Scaling of temporal correlations in an attractive Tomonaga-Luttinger spin liquid,” *Phys. Rev. B* **91**, 020406 (2015).
- [8] J. Ollivier and H. Mutka, “IN5 Cold Neutron Time-of-Flight Spectrometer, Prepared to Tackle Single Crystal Spectroscopy,” *J. Phys. Soc. Jpn.* **80**, SB003 (2011).
- [9] H.-J. Mikeska, U. Neugebauer, and U. Schollwöck, “Spin ladders with nonmagnetic impurities,” *Phys. Rev. B* **55**, 2955–2963 (1997).

- [10] A. Lavarélo, G. Roux, and N. Laflorencie, “Magnetic responses of randomly depleted spin ladders,” *Phys. Rev. B* **88**, 134420 (2013).
- [11] B. Bauer, L. D. Carr, H. G. Evertz, A. Feiguin, J. Freire, S. Fuchs, L. Gamper, J. Gukelberger, E. Gull, S. Guertler, *et al.*, “The ALPS project release 2.0: open source software for strongly correlated systems,” *J. Stat. Mech. Theor. Exp.* **2011**, P05001 (2011).
- [12] M. Dolfi, B. Bauer, S. Keller, A. Kosenkov, T. Ewart, A. Kantian, T. Giamarchi, and M. Troyer, “Matrix product state applications for the {ALPS} project,” *Comput. Phys. Commun.* **185**, 3430 (2014).
- [13] O. F. Syljuåsen and A. W. Sandvik, “Quantum monte carlo with directed loops,” *Phys. Rev. E* **66**, 046701 (2002).
- [14] David Schmidiger, Unpublished.